

DELAY NETWORK ARCHITECTURES FOR ROOM AND COUPLED SPACE MODELING

Orchisama Das, Jonathan S. Abel, Elliot K. Canfield-Dafilou

Center for Computer Research in Music and Acoustics
Stanford University
Stanford, CA, USA

[orchi|abel|kermit]@ccrma.stanford.edu

ABSTRACT

Feedback delay network reverberators have decay filters associated with each delay line to model the frequency dependent reverberation time (T_{60}) of a space. The decay filters are typically designed such that all delay lines independently produce the same T_{60} frequency response. However, in real rooms, there are multiple, concurrent T_{60} responses that depend on the geometry and physical properties of the materials present in the rooms. In this paper, we propose the Grouped Feedback Delay Network (GFDN), where groups of delay lines share different target T_{60} s. We use the GFDN to simulate coupled rooms, where one room is significantly larger than the other. We also simulate rooms with different materials, with unique decay filters associated with each delay line group, designed to represent the T_{60} characteristics of a particular material. The T_{60} filters are designed to emulate the materials' absorption characteristics with minimal computation. We discuss the design of the mixing matrix to control inter- and intra-group mixing, and show how the amount of mixing affects behavior of the room modes. Finally, we discuss the inclusion of air absorption filters on each delay line and physically motivated room resizing techniques with the GFDN.

1. INTRODUCTION

Feedback delay networks (FDNs) are efficient structures for synthesizing room impulse responses (RIRs). RIRs consist of a set of sparse early reflections which increase in density over time, building toward late reverberation where the impulse density is high and statistically Gaussian. Feedback delay networks are composed of delay lines in parallel, which are connected through a feedback matrix (or mixing matrix), which is unitary to conserve system energy [1]. Jot proposed adding shelf filters to the delay lines to yield a desired frequency dependent T_{60} [2, 3]. Since then, FDNs have become one of the most popular structures for synthesizing reverberation due to the relative efficiency of the approach. Recent research on FDNs has focused on mixing matrix design to increase echo density [4], modal analysis [5, 6], time-varying FDNs [7], directional FDNs [8], and reverberation time control by accurate design of the decay filters [9, 10].

In this paper, we propose a new delay network architecture for physically informed room modeling. We also provide an alternate design technique to the one proposed in [10], where a 10-band graphic equalizer consisting of cascaded second order peak-notch

Copyright: © 2020 Orchisama Das, Jonathan S. Abel, and Elliot K. Canfield-Dafilou. This is an open-access article distributed under the terms of the Creative Commons Attribution 3.0 Unported License, which permits unrestricted use, distribution, and reproduction in any medium, provided the original author and source are credited.

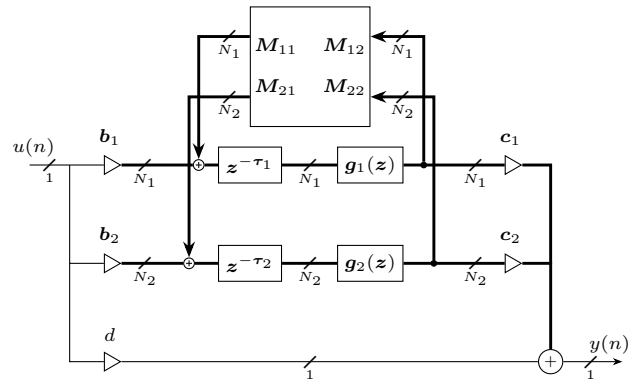


Figure 1: GFDN block diagram.

IIR filters was fit to a desired T_{60} response. Our argument is that the T_{60} response of a room depends on the physical configuration of the room, and room modes at the same frequency need not share the same T_{60} . The T_{60} response of each material depends on its frequency dependent absorption coefficients and its volume to surface area ratio, according to the Sabine theory of late-field reverberation [11]. We propose a new architecture, called the *grouped feedback delay network* (GFDN), where groups of delay lines have the same target T_{60} response associated with them. These filters are designed to be low-order filters consisting of cascaded shelf and resonant biquad filters. Low order filters significantly reduce the computation required in [10], where each delay line has an IIR filter of order 20. The interaction among the different delay line groups is controlled by a block mixing matrix. As applications of the proposed GFDN, we model coupled rooms, a single room composed of different materials, and propose an efficient means of incorporating air absorption and a physically accurate method to resize the modeled rooms.

In §2, we introduce the structure of the GFDN, and discuss block mixing matrix design. In §3, we use the GFDN to simulate the impulse response of a large room coupled with a smaller room, such as box seating in an opera hall. Two different sets of decay filters, associated with two delay line groups are used, and the mixing matrix is parameterized by a coupling coefficient, which effectively controls the amount of coupling between the two rooms. In §4, a single room made of different materials is modeled with the GFDN. Delay line groups have different T_{60} filters associated with each material. T_{60} filter design according to material absorption characteristics is discussed in §4.1. The amount of mixing controls the behavior of the GFDN modes. Modal analysis as a function of the mixing matrix shows how the T_{60} characteristics of different materials interact as occupancy of a room changes

[6]. In §5, we build upon the method proposed in [12] and discuss efficient room resizing with the GFDN by taking into consideration air absorption, delay line lengths and T_{60} filters. The paper is concluded in §6.

2. GROUPED FEEDBACK DELAY NETWORKS

A standard feedback delay network consists of N delay lines of length τ_i seconds $i = 1, 2, \dots, N$, each with its associated decay filter, $g_i(z)$, connected through an $N \times N$ feedback matrix, \mathbf{M} . For a frequency dependent $T_{60}(z)$, the decay filter gains are related to the delay line length as

$$g_i(z) = 0.001 \exp\left(\frac{\tau_i}{T_{60}(z)}\right). \quad (1)$$

The same $T_{60}(z)$ is used to design the decay filters in all N delay lines. In the proposed grouped feedback delay network architecture, we use different $T_{60}(z)$ for each set of delay lines. In Fig. 1, a GFDN with two sets of delay lines are shown. For a total of N delay lines, N_1 delay lines have a decay response, $T_{60_1}(z)$, and N_2 delay lines have a decay response, $T_{60_2}(z)$, such that $N_1 + N_2 = N$. The two groups of decay filter gains, $g_1(z)$ and $g_2(z)$ are calculated according to the different $T_{60}(z)$ s. The mixing matrix \mathbf{M} is now an $N \times N$ block matrix made of the submatrices, $\mathbf{M}_{ij} \in \mathbb{R}^{N_i \times N_j}$, $i, j = 1, 2$. With $\mathbf{c}_i, \mathbf{b}_i, \mathbf{g}_i \in \mathbb{C}^{N_i \times 1}$ and $\tau_i \in \mathbb{R}^{N_i \times 1}$, the transfer function of Fig. 1, $H(z)$, can be written as

$$\begin{aligned} H(z) &= \frac{Y(z)}{U(z)} \\ &= d + [\mathbf{c}_1 \quad \mathbf{c}_2] \left(\begin{bmatrix} \mathbf{g}_1(z)z^{-\tau_1} & \mathbf{0} \\ \mathbf{0} & \mathbf{g}_2(z)z^{-\tau_2} \end{bmatrix} \right. \\ &\quad \left. \left(\mathbf{I} - \begin{bmatrix} \mathbf{g}_1(z)z^{-\tau_1} & \mathbf{0} \\ \mathbf{0} & \mathbf{g}_2(z)z^{-\tau_2} \end{bmatrix} \begin{bmatrix} \mathbf{M}_{11} & \mathbf{M}_{12} \\ \mathbf{M}_{21} & \mathbf{M}_{22} \end{bmatrix} \right)^{-1} \begin{bmatrix} \mathbf{b}_1 \\ \mathbf{b}_2 \end{bmatrix} \right) \end{aligned} \quad (2)$$

The mixing matrix determines the amount of coupling between various delay lines. This property controls the rate at which the echo density increases. A room with many objects and complex geometry will mix faster than an empty room with simple geometry. The mixing matrix can be designed to have a desired mixing time according to the method in [6], where the Kronecker product of a 2×2 rotation/reflection matrix (parameterized by an angle θ) with itself is taken $\log_2(N)$ times to give an $N \times N$ orthonormal matrix, $\mathbf{M}(\theta)$

$$\begin{aligned} \mathbf{R}(\theta) &= \begin{bmatrix} \cos \theta & \sin \theta \\ -\sin \theta & \cos \theta \end{bmatrix} \\ \mathbf{M}_{N \times N}(\theta) &= \mathbf{R}(\theta) \otimes \mathbf{R}(\theta) \otimes \dots \otimes \mathbf{R}(\theta). \end{aligned} \quad (3)$$

A well-diffused room with fast mixing time can be achieved by a scaled Hadamard mixing matrix ($\theta = \frac{\pi}{4}$). Similarly, a ‘‘room’’ with no mixing and no increase in echo density can be synthesized by an Identity mixing matrix ($\theta = 0$). The parameter θ can be chosen to give a desired mixing time, where $\theta = \frac{\pi}{4}$ yields the maximum amount of mixing and smaller positive values give less mixing.

In the GFDN, we can choose different, independent θ values for each delay line group (the diagonal submatrices \mathbf{M}_{11} and

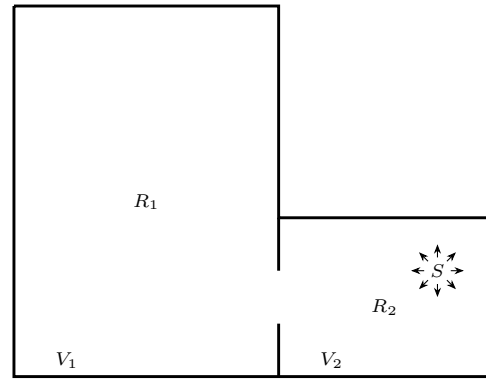


Figure 2: Coupled rooms

\mathbf{M}_{22}). The off-diagonal submatrices (\mathbf{M}_{12} and \mathbf{M}_{21}) then control how strongly coupled the groups are to each other. This gives us independent control over the intra- and inter-group mixing characteristics. The design of these submatrices will be described thoroughly in the following section.

3. COUPLED ROOMS

Two or more rooms can be coupled through an acoustically transparent aperture. If the acoustic source is present in the smaller room with a shorter decay time, the sound will travel to the larger room and spill back into the first room. Such a configuration is shown in Fig. 2. The resulting impulse response will have a non-exponential decay. The first part of the decay has a steeper slope due to the short decay rate of the first room, whereas the latter part has a gentler slope representing the longer decay rate of the second room. This is known as the Double-slope effect (DSE). The physics of sound propagation in coupled rooms was studied in [13]. The effect of the volume ratio, absorption ratio and aperture size on the double slope profile was studied in [14]. Coupled spaces are ubiquitous in the real world. They are found in concert halls, opera halls, and churches [15] where columns, arches, domes, etc., divide the space into two or more subspaces with different absorption properties.

3.1. Coupled mixing matrix design

The mixing matrix is crucial in simulating coupled rooms since it controls diffusion within each room and among the rooms. A method for mixing matrix design in coupled rooms has been suggested in [16], where a sign-agnostic Procrustes method is used to convert an arbitrary matrix to its nearest orthonormal form. Here, we take a different approach. The diagonal submatrices that represent mixing in rooms 1 and 2 respectively can be characterized by two mixing angles, θ_1 and θ_2 depending on the occupancy of the rooms. The off-diagonal matrices represent the coupling between two rooms, and can be represented by matrices $\mathbf{R}_{12}, \mathbf{R}_{21}$, multiplied by a scalar, α , which represents the amount of coupling.

$$\mathbf{M} = \begin{bmatrix} \mathbf{M}(\theta_1) & \alpha \mathbf{R}_{12} \\ \alpha \mathbf{R}_{21} & \mathbf{M}(\theta_2) \end{bmatrix}. \quad (4)$$

This coupled mixing matrix is required to be orthonormal by design. Using this criteria, i.e., $\mathbf{M}^T \mathbf{M} = \mathbf{I}$, we come up with the

following constraints:

1. \mathbf{R}_{12} and \mathbf{R}_{21} need to be orthonormal.
2. $\mathbf{M}(\theta_1)^T \mathbf{R}_{12} + \mathbf{R}_{21}^T \mathbf{M}(\theta_2) = 0 \Rightarrow$

$$\mathbf{R}_{21} = -\mathbf{M}(\theta_2) \mathbf{R}_{12}^T \mathbf{M}(\theta_1).$$
3. \mathbf{M} needs to be scaled by $\frac{1}{\sqrt{1+\alpha^2}}$.

Let $\mathbf{R}_{12} = \mathbf{M}(\theta_1)^{\frac{1}{2}} \mathbf{M}(\theta_2)^{\frac{1}{2}} = \mathbf{M}(\frac{\theta_1}{2}) \mathbf{M}(\frac{\theta_2}{2})$. Therefore, $\mathbf{R}_{21} = -\mathbf{M}(\frac{\theta_2}{2}) \mathbf{M}(\frac{\theta_1}{2})$. Now, the orthonormal mixing matrix is

$$\mathbf{M} = \frac{1}{\sqrt{1+\alpha^2}} \begin{bmatrix} \mathbf{M}(\theta_1) & \alpha \mathbf{M}(\frac{\theta_1}{2}) \mathbf{M}(\frac{\theta_2}{2}) \\ -\alpha \mathbf{M}(\frac{\theta_2}{2}) \mathbf{M}(\frac{\theta_1}{2}) & \mathbf{M}(\theta_2) \end{bmatrix}. \quad (5)$$

Let $\frac{1}{\sqrt{1+\alpha^2}} = \cos \phi$ and $\frac{\alpha}{\sqrt{1+\alpha^2}} = \sin \phi$, then our mixing matrix is characterized by a *coupling angle*, $\phi \in [0, \frac{\pi}{4}]$ radians. When $\phi = 0$, we get minimum coupling (diagonal \mathbf{M}), and when $\phi = \frac{\pi}{4}$, we get maximum coupling between the two rooms. The final parameterized coupled mixing matrix is

$$\mathbf{M}(\theta_1, \theta_2, \phi) = \begin{bmatrix} \cos \phi \mathbf{M}(\theta_1) & \sin \phi \mathbf{M}(\frac{\theta_1}{2}) \mathbf{M}(\frac{\theta_2}{2}) \\ -\sin \phi \mathbf{M}(\frac{\theta_2}{2}) \mathbf{M}(\frac{\theta_1}{2}) & \cos \phi \mathbf{M}(\theta_2) \end{bmatrix}. \quad (6)$$

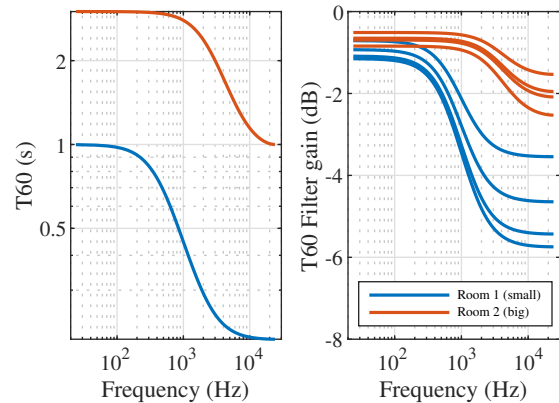
3.2. Evaluation

To simulate coupled rooms, R_1 and R_2 , we design an 8 delay line GFDN, with 4 delay lines each representing the smaller and larger room, with the source placed in R_2 and listener placed in R_1 . The source and listener locations are determined by the $\mathbf{b}_1, \mathbf{b}_2$ and $\mathbf{c}_1, \mathbf{c}_2$ coefficients respectively. The T_{60} filters of the two rooms are first order low shelf filters parameterized by the DC and Nyquist gains and transition frequency. The smaller room, R_1 , (in blue) has a shorter decay time, so its $T_{60}(0) = 1$ s, $T_{60}(\infty) = 0.2$ s and $f_T = 1$ kHz. The larger room, R_2 (in red) has $T_{60}(0) = 3$ s, $T_{60}(\infty) = 1$ s and $f_T = 4$ kHz. The decay filters, $\mathbf{g}_1(z), \mathbf{g}_2(z)$ calculated according to (1) are shown in Fig. 3a.

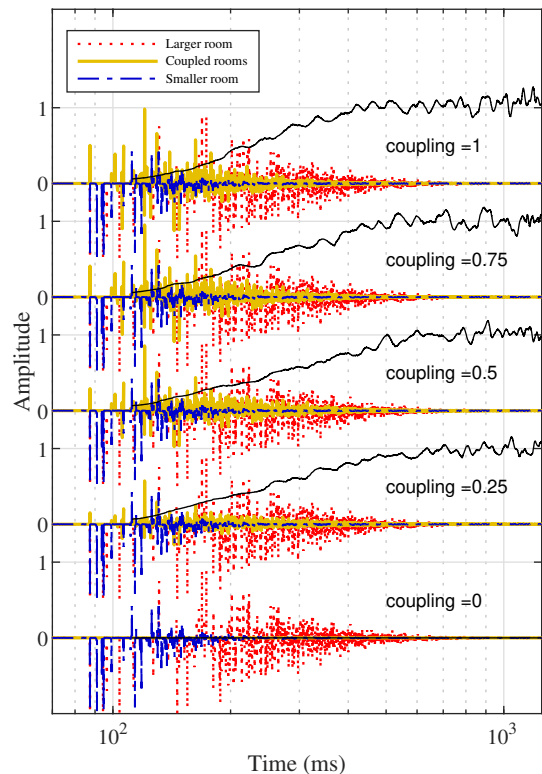
The impulse responses of the coupled GFDN¹ as a function of linearly spaced coupling angles (normalized by $\frac{\pi}{4}$) is shown in Fig. 3b. As expected, when $\phi = 0$, the rooms are decoupled and the GFDN gives zero output. Increasing ϕ increases diffusion between the two rooms, giving denser reverb. The normalized echo density (NED) [17], which is a perceptual measure of reverberation that helps quantify when early decay switches to late reverb, is plotted in black. The NED plots show that denser reverberation is achieved more quickly as ϕ increases. The effect of the smaller room dominates in the coupled room RIRs as ϕ increases. This appears to go against the finding in [14], where subjects of a listening test perceived more reverberance as coupling coefficient increased. However, in our case the source is in the smaller room whereas the listener is in the bigger room. So, the perceived reverberance will decrease as coupling coefficient increases.

Additionally, we calculate the slopes of the two-stage decay of the synthesized RIR. We do this by fitting the sum of two decaying exponentials and a constant to the energy envelope of the

¹All sound examples are available at <https://ccrma.stanford.edu/~orchi/FDN/GFDN/GFDN.html>



(a) Desired T_{60} response (left). Delay line T_{60} filters (right).



(b) Impulse responses for different coupling coefficients. Normalized Echo Density (NED) in black.

Figure 3: Coupled Rooms modeled with GFDN

synthesized RIR

$$h_{env}(t) = \gamma_0 + \gamma_1 \exp\left(-\frac{t}{T_1}\right) + \gamma_2 \exp\left(-\frac{t}{T_2}\right). \quad (7)$$

We use MATLAB's `fmincon` to find the decay rates T_1, T_2 , and update γ using weighted least squares (with more weight on the tail). Two-stage decay of the RIR, with the fitted curve can be seen in Fig. 4a. The ratio of T_{60} s calculated from T_1 and T_2 , as a function of the coupling coefficient, is shown in Fig. 4b. This is known as the *decay ratio* [14]. A larger decay ratio indicates more coupling.

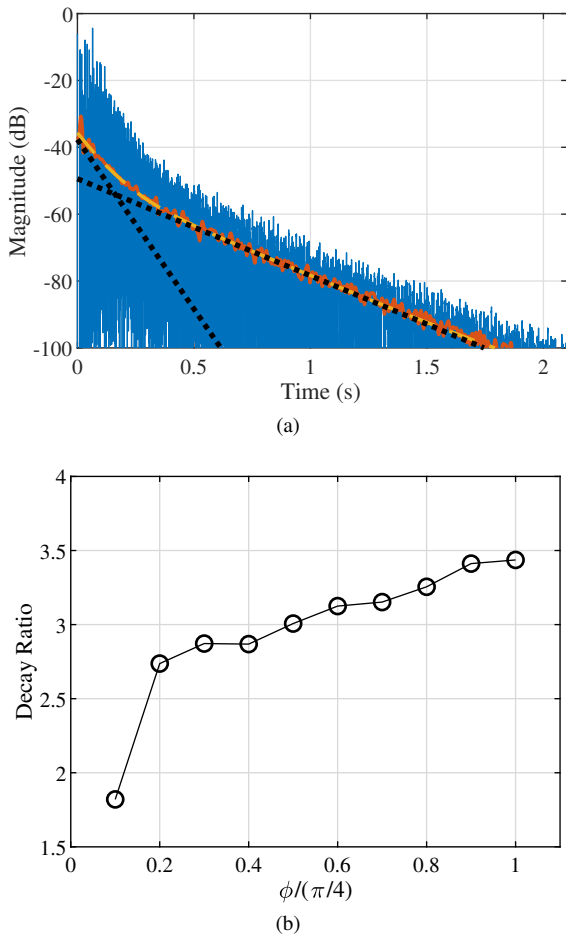


Figure 4: Top - Two-stage decay in coupled GFND impulse response for $\phi = \frac{\pi}{4}$. Red line indicates energy envelope, yellow line is the curve fit and the black dotted lines are the 2-stage decay fits. Bottom - Decay Ratio (ratio of T_{60} s of two rooms) v/s normalized coupling angle.

4. SINGLE ROOM WITH DIFFERENT MATERIALS

As described in [11], the acoustic energy density of a room, $w(t)$, with volume V , and absorbing surface area A , decays exponentially as a function of time

$$\begin{aligned} w(t) &= w_0 e^{-\frac{t}{\tau}} \\ \tau &= \frac{V}{gcA}, \\ T_{60} &= -2 \log(0.001) \tau \end{aligned} \quad (8)$$

where c is the speed of sound, and g is a geometric constant. A room is typically constructed of several absorbing materials, each with its unique frequency dependent absorption $S(\omega)$, and surface area, a . The T_{60} of the room, and of the individual materials is given by

Material	Frequency (Hz)					
	125	250	500	1000	2000	4000
Plywood	0.28	0.22	0.17	0.22	0.10	0.11
Glass	0.35	0.25	0.18	0.12	0.07	0.04
Carpet	0.02	0.06	0.14	0.37	0.66	0.65
Air	0.10	0.30	0.60	1.00	1.90	5.80

Table 1: Absorption coefficients of different materials as function of frequency. Absorption coefficients of air is the ANSI standard at 20° C, 30 – 50% humidity.

$$\begin{aligned} T_{60_{\text{room}}}(\omega) &= -2 \log(0.001) \frac{V}{gc \sum_i a_i S_i(\omega)} \\ T_{60_{\text{mat}_i}}(\omega) &= -2 \log(0.001) \frac{V}{gca_i S_i(\omega)} \end{aligned} \quad (9)$$

To model such a room with the GFDN, we associate different T_{60} filters with each group of delay lines, corresponding to different materials present in the room. Groups of delay lines that share the same T_{60} filter represent surfaces in the room that are made of the same material. T_{60} corresponding to a material depends on the volume to surface area ratio $\frac{V}{a}$, and the materials' absorption characteristics $S(\omega)$. This is unlike standard FDNs, where a single T_{60} filter representing the room's reverberation time is associated with all delay lines. This yields significant computational savings, because T_{60} filters associated with most materials can be represented by simple low order IIR filters. However, a single T_{60} filter based on room geometry (9), would require a very high-order filter. A physical motivation behind this design choice is that in real rooms, multiple modes at the same frequency can have different decay rates, that depend on the properties and distances between surfaces from which the acoustic waves get reflected.

4.1. T60 filter design

By specifying the absorption coefficients and the volume to surface area ratio in a room, T_{60} filters for several materials can be designed. Table 1 shows the absorption coefficients of three common construction materials and air in octave bands. In Fig. 5, filter fits to T_{60} responses of plywood, glass, carpet and air is shown.

Often, (Fig. 5b, 5d), a simple first order shelf filter is enough to model the desired T_{60} response. The first order shelf filter, parameterized by its DC gain, γ_0 , Nyquist gain, γ_π and transition frequency ω_T , is given by

$$H(s) = \sqrt{\gamma_0 \gamma_\pi} \frac{\left(\frac{s}{\omega_T}\right) + \left(\frac{\gamma_0}{\gamma_\pi}\right)^{\frac{1}{2}}}{\left(\frac{s}{\omega_T}\right) \left(\frac{\gamma_0}{\gamma_\pi}\right)^{\frac{1}{2}} + 1} \quad (10)$$

For materials like plywood that have resonant shelf-like T_{60} characteristics (Figs. 5a), we can cascade a peak/notch biquad filter with a first order shelf filter. Thus, a third order filter is needed. The transfer function of the peak (or notch) biquad, parameterized by its peak frequency ω_c , gain at peak frequency γ_{ω_c} and quality factor Q , is given by

$$H(s) = \frac{\left(\frac{s}{\omega_c}\right)^2 + \frac{\gamma_{\omega_c}}{Q} \left(\frac{s}{\omega_c}\right) + 1}{\left(\frac{s}{\omega_c}\right)^2 + \frac{1}{Q} \left(\frac{s}{\omega_c}\right) + 1} \quad (11)$$

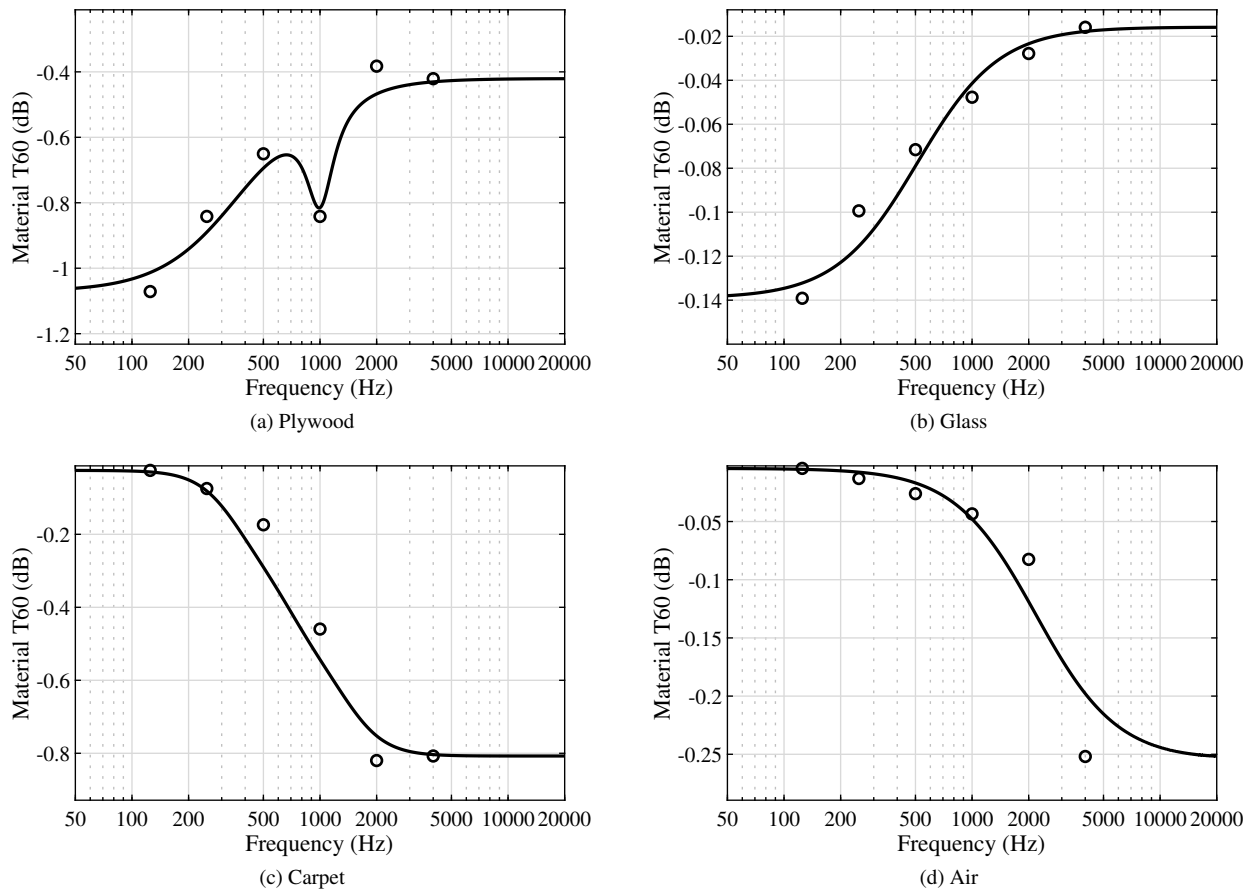


Figure 5: T_{60} filter fits to different materials for a delay line length of 10 ms. Circles represent theoretical T_{60} values calculated according to Sabine’s equation.

The details of converting these analog filter coefficients to digital filter coefficients is given in [18].

Some materials have a steeper T_{60} slope, and a first or second order shelf filter is not enough to model their responses (Fig. 5c). For such materials, we use the method in [19] to cascade multiple second order shelf filters (N_O biquads per octave) to achieve a desired transition bandwidth in number of octaves β , upper cutoff frequency ω_u , DC gain γ_0 , and Nyquist gain γ_π . The total number of biquads needed is $N = \lceil \beta N_O \rceil$. The center frequencies of the N filters are $\omega_{c_\mu} = 2^{-\beta} \omega_u$, and the DC and Nyquist gains of each of the filters is $\gamma_{0,\pi_\mu} = \sqrt[N]{\gamma_0, \gamma_\pi}$. For $Q = \frac{1}{\sqrt{2}}$, the transfer function of the cascaded shelf filters is given by

$$H(s) = \prod_{\mu=0}^{N-1} H_\mu(s)$$

$$H_\mu(s) = \frac{\left(\frac{s}{\omega_{c_\mu}}\right)^2 \gamma_{0_\mu}^{\frac{1}{2}} + \left(\frac{s}{\omega_{c_\mu}}\right) \frac{(\gamma_{0_\mu} \gamma_{\pi_\mu})^{\frac{1}{4}}}{Q} + \gamma_{\pi_\mu}^{\frac{1}{2}}}{\left(\frac{s}{\omega_{c_\mu}}\right)^2 \gamma_{0_\mu}^{-\frac{1}{2}} + \left(\frac{s}{\omega_{c_\mu}}\right) \frac{(\gamma_{0_\mu} \gamma_{\pi_\mu})^{-\frac{1}{4}}}{Q} + \gamma_{\pi_\mu}^{-\frac{1}{2}}}. \quad (12)$$

For designing the T_{60} filter of carpet (Fig. 5c), we chose $\beta = 3$ and $N_O = 1$, giving a total of 3 biquads, and a filter order of 6.

4.2. Evaluation

We synthesize the RIR of a $5 \times 5 \times 5 \text{ m}^3$ cubical room with a carpeted floor (25 m^2), a glass window on a wall (8 m^2), and plywood on the ceiling and rest of the walls (77 m^2) with a 16 delay line GFDN, with 8 delay lines dedicated to modeling plywood, and 4 delay lines for carpet and glass each. We vary the mixing matrix from minimum to maximum occupancy (identity to Hadamard). T_{60} s for smaller mixing angles are longer. The modal decomposition of the GFDN, calculated according to [5], for four different mixing angles is shown in Fig. 6. As per our previous work [6], mode dampings approach each other and mode frequencies repel as mixing increases. This effect is clearly visible, as mode T_{60} responses start by resembling the individual filter characteristics of the three materials for no mixing, but as mixing increases, they scatter towards each other. For a fully mixed GFDN, the T_{60} s are well mixed and converge within a narrow band, thus giving a more diffused RIR.

However, the unusually high T_{60} of the modes produce very long RIRs. This is because we have not taken into account the effect of air absorption in the room, which is discussed in the following section.

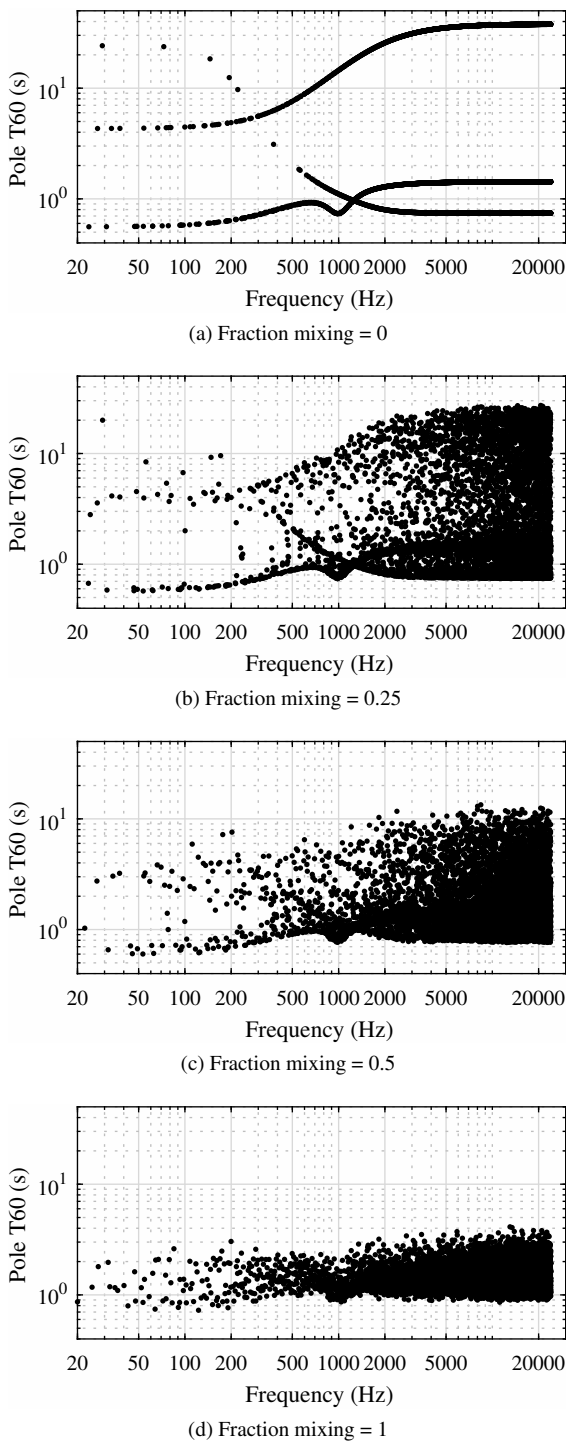


Figure 6: GFDN modes (T_{60} v/s frequency) as function of mixing matrix angle. Increase in mixing causes modes to approach each other in damping and scatter.

5. AIR ABSORPTION AND ROOM RESIZING

As described by Sabine’s equation (8), reverberation time is related to volume and surface area of the room. In small rooms, the reverberation time and characteristic are predominantly a result of the materials properties, but in larger rooms, the effect of air absorption becomes significant as the volume increases. The architecture of the GFDN described above can be useful for realistically modeling rooms of different sizes. In addition to having each delay line group represent a single material, we can cascade an air absorption filter (first-order shelf) with each delay line. Naturally, this increases the filter order for each delay line, however it improves our ability to model the reverberation characteristics of realistic rooms.

Fig. 7 shows the frequency responses of the T_{60} filters, impulse responses, and spectrograms of the room described in §4.2 with and without the effect of air absorption. Since this is a medium sized room, the effect of inclusion of air has a noticeable effect in the damping the high frequencies. The inclusion of air absorption also has a significant effect in making the reverberation sound natural and less metallic.

Now, say we have a GFDN that models a room that we like but we want to increase or decrease the size of the room. Since each delay line encodes the size, materials properties, and ratio of absorbing surface area to volume, we can resize the room by scaling the delay line lengths, τ and recalculating the $g(z)$ filter coefficients to account for the changes in surface area and volume.

Let L_0 be the nominal length of the original room. To scale the size of the room by a factor of L , we proportionally scale the delay line lengths

$$\tau_{\text{scaled}} = \frac{L}{L_0} \tau_{\text{original}} \quad (13)$$

Then, based on the new absorbing surface area, volume, and delay line lengths, we recalculate the target T_{60} s and the $g(z)$ filters for each delay line as described in §4. For small rooms, the material properties will be more significant and in large rooms, air absorption will more significant.

Updating the delay line lengths scales the room mode frequencies and fixes the temporal spacing of the early reflections and mixing time while modifying the filters correctly updates the target frequency dependent T_{60} s for a room of the new volume and surface area. This means that we do not need to modify the mixing matrix. Note that the method for room size control here is a refinement to the methods described in [12] since we explicitly have filters for materials and air absorption in each delay line. If real-time room size control is desired, we can forgo modifying the delay line lengths to avoid pitch shift artifacts. Moreover, if we start with the geometry of the room we are modeling, it is easy to scale the dimensions independently. For example, we can raise the roof by modifying the delay line lengths associated with the room’s height only. We have to modify the $g(z)$ filters associated with air absorption since the room’s volume is changed, however we only need to change the materials filters associated with the changes to the surface area of the walls as the floor and ceiling do not change. Alternatively, we do not need to explicitly know the geometry of the room. Since we group some delay lines together, we can modify individual groups to modify different components of the room *abstractly*.

Fig. 8 shows the impulse response, modes, and spectrogram for the GFDN designed for the medium sized room described in §4.2. We additionally show impulse responses and spectrograms

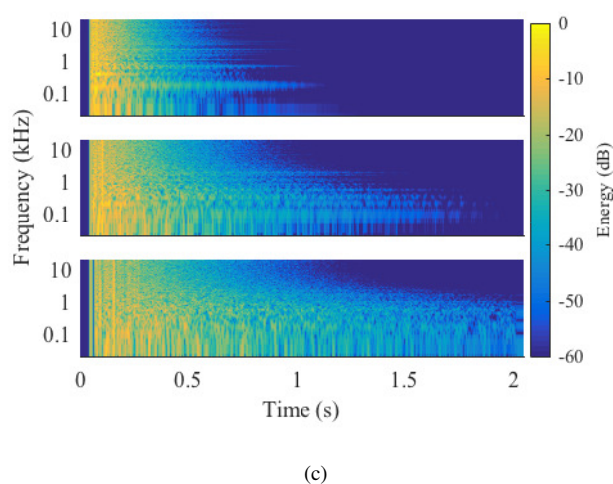
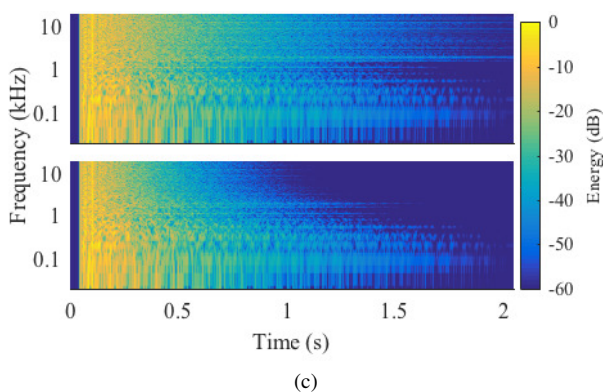
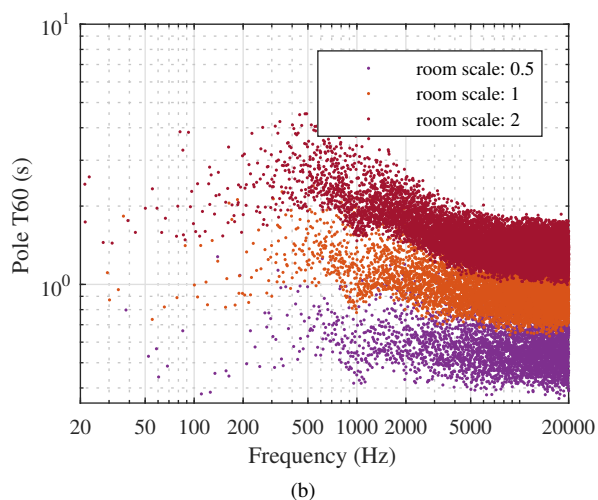
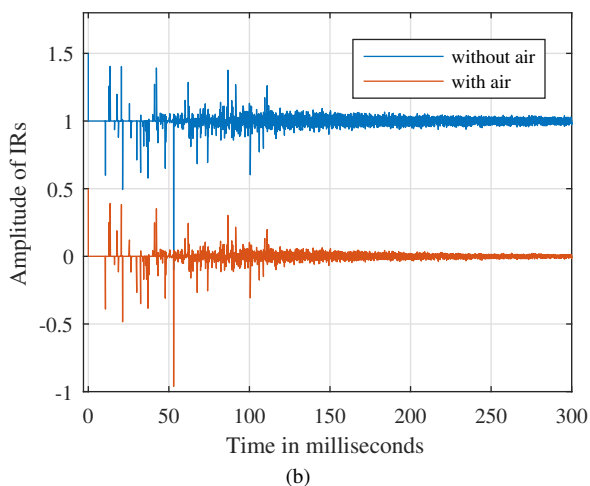
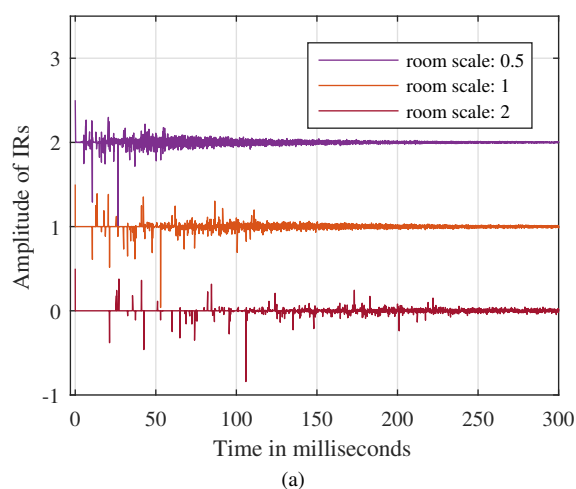
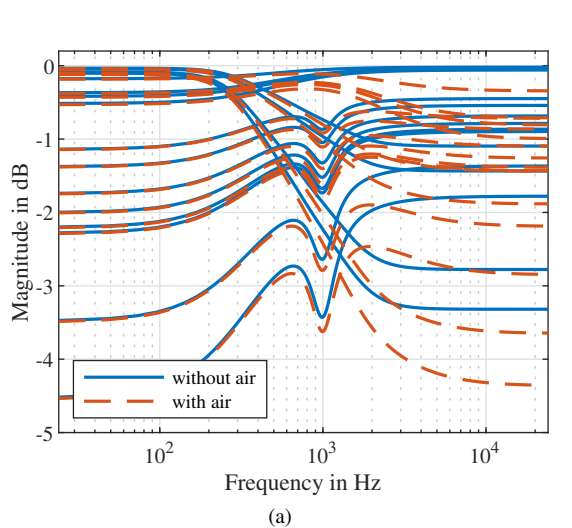


Figure 7: Top - T_{60} filter responses of a GFDN designed to model a medium sized room without and with air absorption. Eight delay lines are used to model plywood, four for carpet, and four for glass. Middle - impulse responses of the GFDN without and with air absorption. Bottom - spectrograms of the GFDN without and with air absorption.

Figure 8: Top - impulse responses of a GFDN designed to model a medium sized room and scaled to have its nominal length halved and doubled. Middle - modes of the same rooms. Bottom - spectrograms of the same rooms.

of the same room, scaled to have the nominal length halved and doubled. One can clearly see how the room sizing operation effects the mode frequencies, early reflection spacing, mixing time, and frequency dependent T_{60} s.

6. CONCLUSION

In this paper, we have proposed the Grouped Feedback Delay Network, which has different decay filters in different groups of delay lines, motivated by the fact that in real rooms neighboring modes do not have a single T_{60} . Instead, they are distributed in a band. We have used the GFDN to synthesize RIRs of coupled rooms, where one room is significantly larger than the other. We have also discussed the design of a parameterized orthonormal coupled mixing matrix that controls the occupancy of the individual rooms and amount of coupling between them. Single rooms composed of different materials (or different absorbing surfaces) have been modeled with the GFDN. Delay line attenuation filters have been designed to represent T_{60} characteristics of different absorbing materials in the room, instead of the space as a whole. Unlike [10], our filters are of a lower order than a 10-band GEQ; hence the GFDN is computationally more efficient. Modal analysis has shown that the mode T_{60} s of the synthesized RIRs follow the individual groups' decay response when there is no mixing, and approach each other as mixing increases, as previously investigated in [6]. Finally, we have discussed the effect of air absorption in attenuating the overall T_{60} response of the modeled room. Methods for room resizing by altering the delay line lengths and decay filter gains have been proposed. We have provided relevant sound examples wherever applicable.

The GFDN cannot be used to exactly match the measured T_{60} response of a particular space. However, it is a cheap way to generate approximate, physically informed RIRs when the configuration of the room is known. Therefore, we think it will find applications in VR audio, where cheap, approximate and dynamic artificial reverberation is a requirement. Perceptual evaluation of GFDN RIRs with those synthesized by ray-tracing/image-source/FDTD methods is a topic we leave open for future work.

7. ACKNOWLEDGEMENT

The authors would like to thank Sebastian J. Schlecht for sharing his FDN Toolbox [20] written in MATLAB, which was used to implement FDN modal analysis with the Ehrlich-Aberth algorithm.

8. REFERENCES

- [1] Michael A. Gerzon, "Unitary (energy-preserving) multi-channel networks with feedback," *Electron. Lett.*, vol. 12, no. 11, pp. 278–279, 1976.
- [2] Jean-Marc Jot and Antoine Chaigne, "Digital delay networks for designing artificial reverberators," in *Proc. Audio Eng. Soc. Conv. 90*, 1991.
- [3] Jean-Marc Jot, "An analysis/synthesis approach to real-time artificial reverberation," in *IEEE Int. Conf. Acoust., Speech, Signal Process.*, 1992, vol. 2, pp. 221–224.
- [4] Sebastian J. Schlecht and Emanuël A. P. Habets, "Dense reverberation with delay feedback matrices," in *IEEE Workshop Appl. Signal Process. Audio Acoust.*, 2019, pp. 150–154.
- [5] Sebastian J. Schlecht and Emanuël A. P. Habets, "Modal decomposition of feedback delay networks," *IEEE Trans. Signal Process.*, vol. 67, no. 20, pp. 5340–5351, 2019.
- [6] Orchisama Das, Elliot K. Canfield-Dafilou, and Jonathan S. Abel, "On the behavior of delay network reverberator modes," in *IEEE Workshop Appl. Signal Process. Audio Acoust.*, 2019, pp. 50–54.
- [7] Sebastian J. Schlecht and Emanuël A. P. Habets, "Time-varying feedback matrices in feedback delay networks and their application in artificial reverberation," *J. Acoust. Soc. Amer.*, vol. 138, no. 3, pp. 1389–1398, 2015.
- [8] Benoit Alary, Archontis Politis, Sebastian J. Schlecht, and Vesa Välimäki, "Directional feedback delay network," *J. Audio Eng. Soc.*, vol. 67, no. 10, pp. 752–762, 2019.
- [9] Sebastian J. Schlecht and Emanuël A. P. Habets, "Accurate reverberation time control in feedback delay networks," *Int. Conf. Digit. Audio Effects*, pp. 337–344, 2017.
- [10] Karolina Prawda, Vesa Välimäki, Sebastian J. Schlecht, et al., "Improved reverberation time control for feedback delay networks," in *Int. Conf. Digit. Audio Effects*, 2019.
- [11] Wallace C. Sabine, *Collected papers on acoustics*, Peninsula Publishing, Los Alto, CA, 1993.
- [12] Elliot K. Canfield-Dafilou and Jonathan S. Abel, "Resizing rooms in convolution, delay network, and modal reverberators," in *Int. Conf. Digit. Audio Effects*, 2018.
- [13] Carl F. Eyring, "Reverberation time measurements in coupled rooms," *J. Acoust. Soc. Amer.*, vol. 3, no. 2A, pp. 181–206, 1931.
- [14] David T. Bradley and Lily M. Wang, "The effects of simple coupled volume geometry on the objective and subjective results from nonexponential decay," *J. Acoust. Soc. Amer.*, vol. 118, no. 3, pp. 1480–1490, 2005.
- [15] John S. Anderson and Magdalena Bratos-Anderson, "Acoustic coupling effects in st paul's cathedral, london," *J. Sound Vib.*, vol. 236, no. 2, pp. 209–225, 2000.
- [16] Sebastian J. Schlecht and Emanuël A. P. Habets, "Sign-agnostic matrix design for spatial artificial reverberation with feedback delay networks," in *Proc. Audio Eng. Soc. Int. Conf. Spatial Reproduction-Aesthetics Sci.*, 2018.
- [17] Jonathan S. Abel and Patty Huang, "A simple, robust measure of reverberation echo density," in *Audio Eng. Soc. Conv. 121*, 2006.
- [18] Julius O. Smith, *Physical Audio Signal Processing*, <http://ccrma.stanford.edu/jos/pasp/>, 2010.
- [19] Frank Schultz, Nara Hahn, and Spors Sascha, "Shelving filter cascade with adjustable transition slope and bandwidth," in *Audio Eng. Soc. Conv. 148*, 2020.
- [20] Sebastian J. Schlecht, "FDNTB: The Feedback Delay Network Toolbox," in *Proceedings of the 23-rd Int. Conf. on Digital Audio Effects (DAFx2020)*, G. Evangelista, Ed., Sept. 2020, vol. 1.